

Article

Effects of Cu Species on Liquid-Phase Partial Oxidation of Methane with H₂O₂ over Cu-Fe/ZSM-5 Catalysts

Min Sik Kim ^{1,†}, Gun Sik Yang ^{1,†} and Eun Duck Park ^{1,2,*} ¹ Department of Energy Systems Research, Ajou University, Suwon 16499, Korea² Department of Chemical Engineering, Ajou University, Suwon 16499, Korea

* Correspondence: edpark@ajou.ac.kr; Tel.: +82-31-219-2384; Fax: +82-31-219-1612

† These authors contributed equally to this work.

Abstract: In this study, a Cu-promoted Fe/ZSM-5 catalyst was examined to reveal the effects of Cu species in selective oxidation of methane into methane oxygenates using H₂O₂ in water. Cu/ZSM-5, Cu-Fe/ZSM-5, and Fe/ZSM-5 catalysts were prepared using wet impregnation, solid-state ion exchange, and ion-exchange methods. Various techniques, including nitrogen physisorption, temperature-programmed reduction with H₂, UV-vis spectroscopy, and FT-IR spectroscopy after NO adsorption, were utilized to characterize the catalysts. The promotional effect of Cu on the Cu-Fe/ZSM-5 catalyst in terms of methanol selectivity was confirmed. The preparation method has a considerable influence on the catalyst performance, and the ion-exchange method is the most effective. However, leaching of the Cu species was observed during this reaction, which can affect the quantification of formic acid by ¹H-NMR. The homogeneous Cu species increase hydrogen peroxide decomposition and CO₂ selectivity, which is undesirable for this reaction.

Keywords: partial oxidation of methane; hydrogen peroxide; Cu-Fe/ZSM-5; methanol; formic acid



Citation: Kim, M.S.; Yang, G.S.; Park, E.D. Effects of Cu Species on Liquid-Phase Partial Oxidation of Methane with H₂O₂ over Cu-Fe/ZSM-5 Catalysts. *Catalysts* **2022**, *12*, 1224. <https://doi.org/10.3390/catal12101224>

Academic Editor: Giuseppe Pantaleo

Received: 19 September 2022

Accepted: 10 October 2022

Published: 13 October 2022

Publisher's Note: MDPI stays neutral with regard to jurisdictional claims in published maps and institutional affiliations.



Copyright: © 2022 by the authors. Licensee MDPI, Basel, Switzerland. This article is an open access article distributed under the terms and conditions of the Creative Commons Attribution (CC BY) license (<https://creativecommons.org/licenses/by/4.0/>).

1. Introduction

The direct conversion of methane into platform chemicals has attracted interest as it can resolve the problem inherent in the indirect methane conversion method, in which methane is first transformed into syngas (CO + H₂) through an energy-intensive process, followed by subsequent chemical conversion processes to synthesize value-added chemicals [1]. In contrast with the indirect methane conversion process, which requires a mega plant for economic feasibility, direct methane conversion can be applied to small-scale natural gas sources if successfully developed. Methane has been principally used as an energy source, but it is also an attractive chemical feedstock as it is cleaner and more abundant than the present chemical feedstocks including petroleum [2]. Therefore, various routes for the direct conversion of methane into value-added products have been proposed and studied [3–9].

The selective oxidation of methane into methane oxygenates containing methanol, formaldehyde, and formic acid is a promising candidate for direct methane conversion technologies because it is thermodynamically and kinetically feasible [10]. It can be performed in gas [11] and liquid phases [12], and at present, different catalyst systems exist. In contrast with the gas-phase partial oxidation of methane, the liquid-phase has been reported to provide high product yields, especially when using strong oxidizing agents (e.g., SO₃ [13,14] and K₂S₂O₈ [15]) in protic solvents such as sulfuric acid [16–18] and trifluoroacetic acid [19,20]. As eco-friendly chemical processes are preferred, selective methane oxidation in an aqueous phase with hydrogen peroxide is being actively investigated [21]. As methane can be selectively transformed into methanol via enzymatic reactions in nature, soluble and particulate methane monooxygenase systems have been investigated and applied to design biomimetic catalyst systems which is more practical than the enzyme itself [22,23]. One of these systems is the metal-incorporated confined system, in which metal

ions and metal oxide clusters can be stabilized inside zeolites [24], carbon materials [25] and metal organic frameworks [26]. This system has reportedly been active in selective methane oxidation with H_2O_2 in liquid water [27–34].

Methanol is the most desirable product among the methane oxygenates formed during this reaction as it can be transformed into other platform chemicals (e.g., olefins and acetic acid) and fuels through well-developed chemical processes (e.g., methanol-to-olefin [35], methanol-to-gasoline [36], and Monsanto [37] processes). Therefore, the development of catalysts for the selective oxidation of methane into methanol has been an important task in the catalyst industry. Hutchings et al. [38] first reported elevated catalytic activity for the partial oxidation of methane with H_2O_2 in water over Fe-ZSM-5 containing 0.017 wt% Fe. Furthermore, they reported that Cu-promoted Fe-ZSM-5 catalysts were active in the selective oxidation of methane into methanol. In addition, they reported that the methanol yield increased when homogeneous $\text{Cu}(\text{NO}_3)_2$ was used with Fe-ZSM-5. However, the opposite observation was reported by Al-Shihri et al. [39] who showed that the methanol yield decreased over Fe-ZSM-5 with increasing quantities of $\text{Cu}(\text{NO}_3)_2$. Recently, Yu et al. [40] achieved a high methanol yield over a Cu-Fe/ZSM-5 catalyst with a relatively greater quantity of Cu than that of Fe. They proposed that the Cu species generated $\bullet\text{OH}$ from H_2O_2 , and methanol could be formed through the reaction between $\bullet\text{OH}$ and $\bullet\text{CH}_3$. Until now, ZSM-5 has been mainly reported to be an effective host material for Fe and/or Cu species for low-temperature aqueous-phase selective oxidation of methane. Recently, we observed that the presence of homogeneous Cu species inhibits the quantification of HCOOH in the product solution using $^1\text{H-NMR}$ spectroscopy, which has been mostly used for the analysis of methane oxygenates in previous research, which prompted the reexamination of this catalyst system.

In this study, the role of Cu species in the partial oxidation of methane was investigated by evaluating the performance of Cu/ZSM-5, Cu-Fe/ZSM-5, and Fe/ZSM-5 catalysts prepared using solid-state ion exchange (SIE), wet impregnation (WI), and ion-exchange (IE) methods. The effect of homogeneous Cu species on the catalytic performance in the absence and presence of Fe/ZSM-5 was also investigated.

2. Results and Discussion

2.1. Physicochemical Properties of the Prepared Catalysts

The textural properties of the prepared catalysts, determined from N_2 physisorption data (Figure S1), are summarized in Table 1. As the metal content of each catalyst was low, the BET surface area, pore volume, micropore area, and micropore volume of each catalyst were slightly smaller than those of the parent H-ZSM-5. There was no noticeable difference among the textural properties of catalysts prepared using the different methods. The X-ray diffraction (XRD) patterns (Figure S2) and transmission electron microscopy (TEM) image with energy-dispersive X-ray spectroscopy (EDS) mapping results (Figure S3) reveal that there is no metal oxide cluster in the prepared catalysts.

The UV-Vis spectra of all catalysts are displayed in Figure 1. Evident peaks were observed at 250 nm and 300 nm for Fe/ZSM-5(IE). The peak intensities of these bands decreased for Fe/ZSM-5(WI), and only a small peak at 300 nm being was observed for Fe/ZSM-5(SIE). However, a more notable, broad peak was observed at >400 nm for Fe/ZSM-5(WI) and Fe/ZSM-5(SIE) compared with that of Fe/ZSM-5(IE). A similar trend was observed for the Cu-Fe/ZSM-5 catalysts. The decreasing trend for the band intensity at 300 nm was Cu-Fe/ZSM-5(IE) $>$ Cu-Fe/ZSM-5(WI) $>$ Cu-Fe/ZSM-5(SIE). However, there were no observable differences in the UV-Vis spectra at >450 nm. A comparison of the UV-Vis spectra of Fe/ZSM-5 and Cu-Fe/ZSM-5 indicated that the peak intensity at >450 nm was weakened by the addition of Cu to Fe/ZSM-5, regardless of the preparation method. All the Cu/ZSM-5 catalysts showed an intense peak at 200 nm and a weak and broad peak at >600 nm, irrespective of the preparation method. All catalysts containing Fe species had an observed main band at 250–350 nm in the UV-Vis spectra, which implied that the isolated Fe species in the extra-framework of the zeolite were dominant [41,42]. Peak deconvolution

was performed to quantify the fraction of each Fe species in the catalysts. Figure S4 and Table S1 indicate that the IE method was the most effective for forming isolated Fe species in the zeolite extra-framework. In the case of Cu-containing catalysts, two typical bands were observed at 200 nm ($50,000\text{ cm}^{-1}$) and 800 nm ($12,500\text{ cm}^{-1}$), which corresponded to the charge-transfer transition and d-d transition of Cu^{2+} ions, respectively [43,44].

Table 1. The textural properties of the prepared catalysts.

Catalyst	Cu Content ^a (wt.%)	Fe Content ^a (wt.%)	BET Surface Area ^b (m ² /g)	Pore Volume ^b (cm ³ /g)	Micropore Area ^c (m ² /g)	Micropore Volume ^c (cm ³ /g)
H-ZSM-5	-	0.01	355	0.20	280	0.12
1.12%Cu/ZSM-5(SIE)	1.12	0.01	304	0.21	198	0.09
0.54%Cu-0.56%Fe/ZSM-5(SIE)	0.54	0.56	305	0.20	204	0.09
0.65%Fe/ZSM-5(SIE)	-	0.65	368	0.23	268	0.12
1.13%Fe/ZSM-5(SIE)	-	1.13	311	0.21	202	0.09
0.99%Cu/ZSM-5(WI)	0.99	0.01	292	0.19	206	0.08
0.55%Cu-0.46%Fe/ZSM-5(WI)	0.55	0.46	287	0.19	206	0.09
0.54%Fe/ZSM-5(WI)	-	0.54	300	0.27	204	0.09
1.05%Fe/ZSM-5(WI)	-	1.05	301	0.21	191	0.09
1.20%Cu/ZSM-5(IE)	1.20	0.01	318	0.20	237	0.11
0.56%Cu-0.30%Fe/ZSM-5(IE)	0.56	0.30	314	0.24	206	0.09
0.51%Fe/ZSM-5(IE)	-	0.51	315	0.26	208	0.10
0.94%Fe/ZSM-5(IE)	-	0.94	311	0.24	211	0.10

^a The metal content was determined with ICP-OES. ^b The BET surface area and pore volume were measured with N₂ physisorption. ^c These data were calculated with t-plot method.

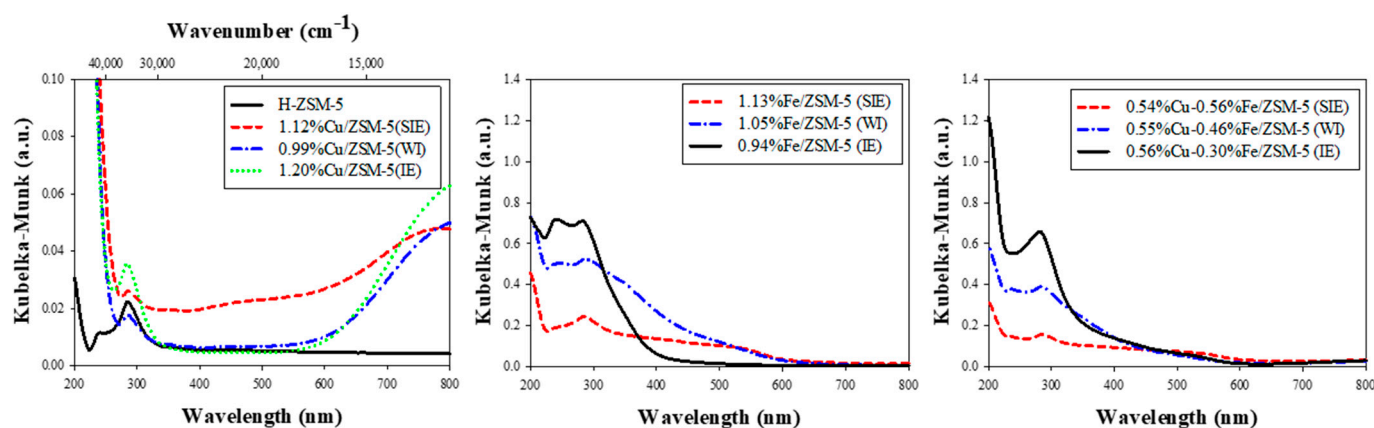


Figure 1. UV-Vis spectra of the catalysts prepared with different methods.

Figure 2 shows the temperature-programmed reduction with H₂ (H₂-TPR) patterns for each catalyst prepared using the different methods. A sharp and well-defined H₂-TPR peak was observed at 185 °C for Cu/ZSM-5(SIE). This peak's intensity was significantly attenuated for Cu/ZSM-5(WI). In contrast, Cu/ZSM-5(IE) showed broad and well-defined peaks with maxima at 175 °C and 380 °C. In the case of the Fe/ZSM-5 catalysts, Fe/ZSM-5(SIE) exhibited two H₂-TPR peaks at 310 and 380 °C. The first low-temperature H₂-TPR peak was much smaller than the second. In contrast, only a single broad H₂-TPR peak was observed at 310 °C for Fe/ZSM-5(WI). A weak and broad H₂-TPR peak was obtained in the temperature range 140–400 °C for Fe/ZSM-5(IE). For the Cu-Fe/ZSM-5 catalysts, different H₂-TPR patterns were obtained for each catalyst. However, H₂-TPR patterns for Cu/ZSM-5 and Fe/ZSM-5 were observed in the H₂-TPR pattern for Cu-Fe/ZSM-5 prepared using the same method. The H₂-TPR pattern was used to probe the surface Cu species on Cu/ZSM-5. It

has been previously reported that CuO, Cu²⁺, and Cu⁺ in zeolites were reduced at 200, 300, and 600 °C, respectively [45]. As shown in Figure 2, Cu/ZSM-5(SIE) and Cu/ZSM-5(IE) were predominantly CuO and Cu²⁺ species, respectively. In the case of Fe-ZSM-5, it has been previously reported that Fe³⁺, Fe_xO_y, and Fe₂O₃ were reduced at 300, 400, and 500 °C, respectively [46,47]. Therefore, Fe/ZSM-5(SIE) has relatively high fractions of Fe_xO_y and Fe₂O₃ content. Contrastingly, Fe/ZSM-5(WI) and Fe/ZSM-5(IE) contained large fractions of Fe³⁺ species. Since the Cu-Fe/ZSM-5 catalysts show the H₂-TPR peaks observed for both Cu/ZSM-5 and Fe/ZSM-5, all Cu and Fe species found in Cu/ZSM-5 and Fe/ZSM-5 appear to be present in Cu-Fe/ZSM-5. Consequently, Cu-Fe/ZSM-5(IE) has the highest fraction of Cu²⁺ and Fe³⁺ species among Cu-Fe/ZSM-5 catalysts.

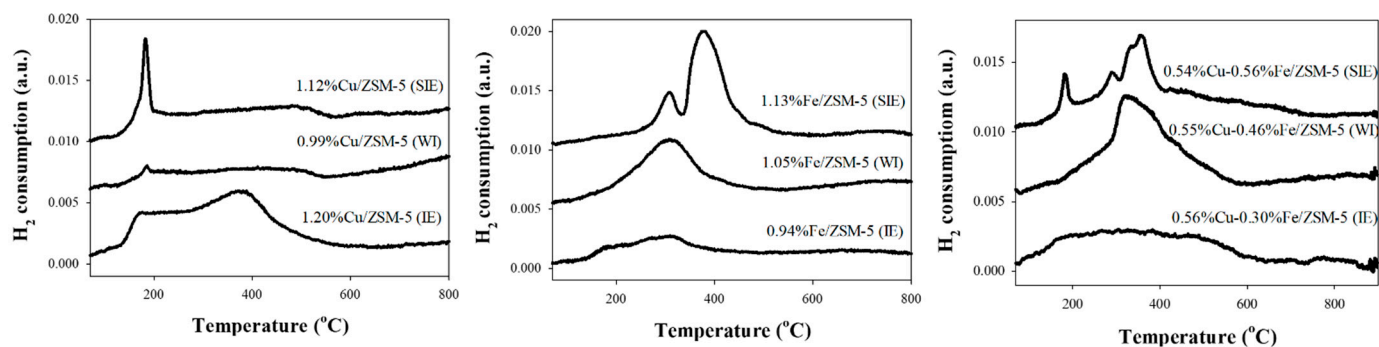


Figure 2. H₂-TPR pattern of the catalysts prepared with different methods.

To elucidate the Fe and Cu species in each catalyst, the IR spectra were obtained after NO adsorption. As shown in Figure 3 and Figure S5, two IR peaks were observed at 1810 and 1910 cm⁻¹ for Cu/ZSM-5(IE). An IR peak at 1910 cm⁻¹ was also observed for Cu/ZSM-5(WI) and Cu/ZSM-5(SIE), but the peak intensity was attenuated compared to that of Cu/ZSM-5(IE). Interestingly, no noticeable IR peak at 1810 cm⁻¹ were observed for Cu/ZSM-5(WI) and Cu/ZSM-5(SIE). In the case of Fe/ZSM-5, two typical IR peaks with different intensities were observed at 1810 and 1880 cm⁻¹ for all catalysts. The decreasing peak intensity order was Fe/ZSM-5(IE) > Fe/ZSM-5(WI) > Fe/ZSM-5(SIE). The IR peaks observed for Cu/ZSM-5 and Fe/ZSM-5 were also observed for Cu-Fe/ZSM-5. The descending order of peak intensities at 1810 and 1880 cm⁻¹ was: Cu-Fe/ZSM-5(IE) > Cu-Fe/ZSM-5(WI) > Cu-Fe/ZSM-5(SIE). In contrast, at 1910 cm⁻¹ the decreasing peak intensity order was: Cu-Fe/ZSM-5(IE), Cu-Fe/ZSM-5(SIE), and Cu-Fe/ZSM-5(WI). FT-IR spectra after NO chemisorption have frequently been used to probe the surface Cu and Fe species in zeolites. The band at 1880 cm⁻¹, which is due to Fe²⁺-(NO) (γ -position), has been reported to be an active Fe species [48–53]. Previous studies regarding Cu/ZSM-5 [44,54–56] have indicated that the 1910 and 1810 cm⁻¹ bands are a result of Cu²⁺-(NO) and Cu⁺-(NO), respectively. Figure 3 shows that Cu/ZSM-5(IE) had dominant Cu⁺-(NO) and Cu²⁺-(NO), in contrast with those Cu/ZSM-5(WI) and Cu/ZSM-5(SIE). The Cu⁺ observed in Cu/ZSM-5(IE) can be formed through the auto-reduction of Cu²⁺, which has been frequently reported in previous EPR and IR studies [54–56]. The band at 1880 cm⁻¹ might be ascribed to Cu²⁺-(NO), which has been reported to occur when the Cu/Al ratio is elevated in Cu/ZSM-5 content (Cu/Al > 0.5) [44,55]. However, because Cu/ZSM-5 has a very low Cu/Al ratio of 0.2, the band at 1880 cm⁻¹ observed for Cu-Fe/ZSM-5 is due to Fe²⁺-(NO) and not Cu²⁺-(NO). The band at 1910 cm⁻¹ may be due to the presence of Fe²⁺-(NO)₂ species. However, this band was not observed for Fe/ZSM-5 catalysts. Therefore, the band at 1910 cm⁻¹ is due to Cu²⁺-(NO). Among the Cu-Fe/ZSM-5 catalysts, Cu-Fe/ZSM-5(IE) showed the largest bands at 1810, 1880, and 1910 cm⁻¹. Consequently, the IE method is the most effective method for dispersing Cu²⁺ and Fe²⁺ species in zeolites.

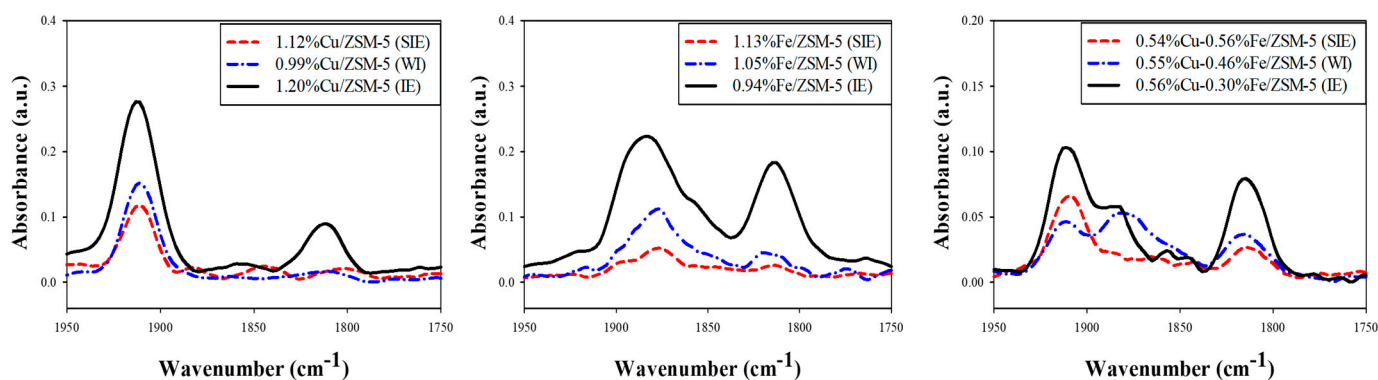


Figure 3. NO-FTIR of the catalysts prepared with different methods.

2.2. Catalytic Activity in a Batch Reactor

The aqueous-phase oxidation of methane with H_2O_2 was performed, and the product yields with hydrogen peroxide conversions over the prepared catalysts at 30 and 50 °C are displayed in Figure 4A and 4B, respectively. Irrespective of the preparation method, Fe/ZSM-5 and Cu/ZSM-5 exhibited the maximum and minimum total product yields, respectively. Furthermore, the ion-exchange method was confirmed to be the most effective preparation method, providing the highest total product yield among the Fe/ZSM-5 and Cu-Fe/ZSM-5 catalysts. Cu-Fe/ZSM-5 showed the highest methanol yield among the tested catalysts, irrespective of the preparation method.

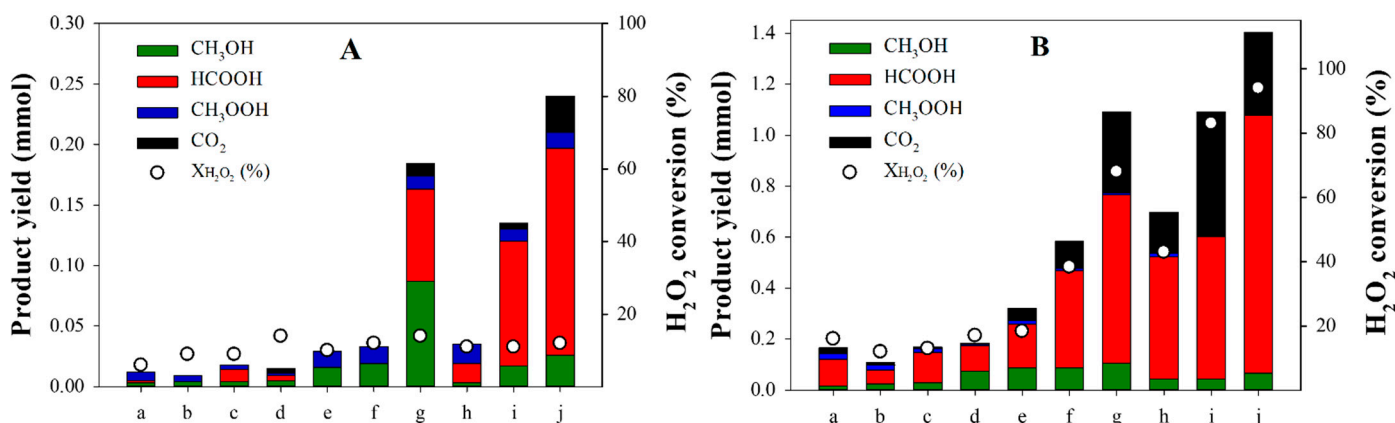


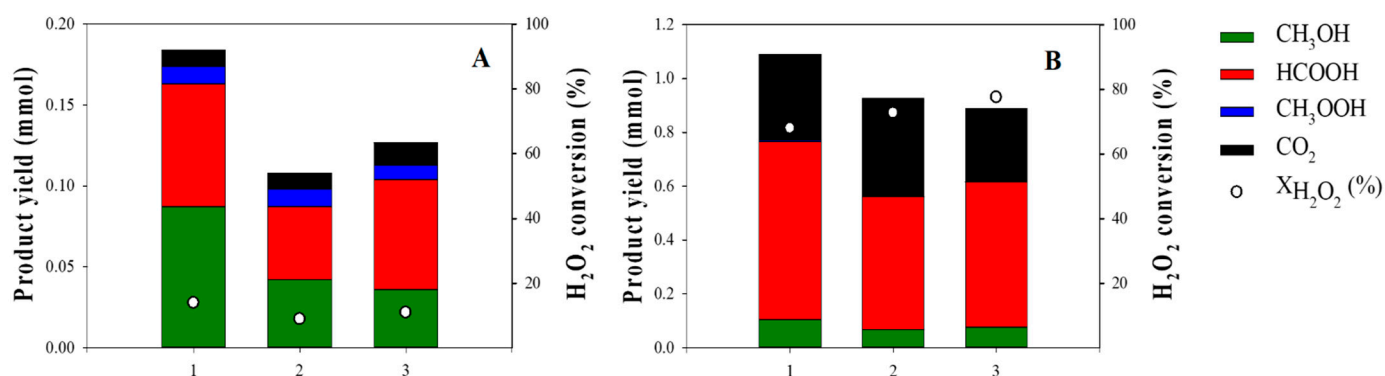
Figure 4. Partial oxidation of methane over H-ZSM-5 (a), 1.12%Cu/ZSM-5(SIE) (b), 0.99%Cu/ZSM-5(WI) (c), 1.20%Cu/ZSM-5(IE) (d), 0.54%Cu-0.56%Fe/ZSM-5(SIE) (e), 0.55%Cu-0.46%Fe/ZSM-5(WI) (f), 0.56%Cu-0.30%Fe/ZSM-5(IE) (g), 1.13%Fe/ZSM-5(SIE) (h), 1.05%Fe/ZSM-5(WI) (i), and 0.94%Fe/ZSM-5(IE) (j). Reaction conditions: 50 mg catalyst, 31 bar methane, 0.277 M H_2O_2 , liquid volume = 30 mL, reaction temperature = 30 °C (A), 50 °C (B).

The Cu content in the liquid phase after the reaction with Cu-containing catalysts was measured. The fractions of Cu leached per total amount of Cu for different catalysts after the reaction are listed in Table 2. At least 10% of Cu was leached from Cu/ZSM-5. In the case of Cu-Fe/ZSM-5, greater fractions of Cu were leached compared to that of Cu/ZSM-5. As the Cu species in Cu/ZSM-5 and Cu-Fe/ZSM-5 were not stable under the reaction conditions, a recycling test was conducted for the Cu-Fe/ZSM-5(IE) catalyst. As shown in Figure 5, the total product yield decreased slightly after the first recycle, although the H_2O_2 conversion did not noticeably change. The fraction of leached Cu relative to the initial total Cu content also increased slightly from 55 to 85% with the number of cycles increasing from 1 to 3.

Table 2. The fraction of Cu leached after a reaction over Cu/ZSM-5 and Cu-Fe/ZSM-5 catalysts ^a.

Entry	Catalyst	The Fraction of Cu Leached
1	1.12%Cu/ZSM-5(SIE)	0.27
2	0.99%Cu/ZSM-5(WI)	0.37
3	1.20%Cu/ZSM-5(IE)	0.13
4	0.54%Cu-0.56%Fe/ZSM-5(SIE)	0.47
5	0.55%Cu-0.46%Fe/ZSM-5(WI)	0.55
6	0.56%Cu-0.30%Fe/ZSM-5(IE)	0.55

^a Reaction conditions: 30 mL of 0.277 M H₂O₂ solution, 95 mL of CH₄ at 31 bar, 50 mg of catalyst, reaction temperature = 50 °C, reaction time = 1 h.

**Figure 5.** The recycle test with 0.56%Cu-0.30%Fe/ZSM-5(IE) at 30 °C (A) and 50 °C (B). Reaction conditions: 50 mg catalyst, 31 bar methane, 0.277 M H₂O₂, liquid volume = 30 mL.

To determine the effect of homogeneous Cu species, various homogeneous Cu catalysts were added to the Fe/ZSM-5(IE) system. As shown in Figure 6, the total product yield decreased, but H₂O₂ conversion increased in the presence of an additional homogeneous Cu catalyst compared to the case with only Fe/ZSM-5(IE). Other heterogeneous copper oxides (e.g., CuO and Cu₂O) and homogeneous Cu catalysts (Cu(CH₃COO)₂, Cu(NO₃)₂, and CuSO₄) were used in this reaction. As shown in Table S2, very small amounts of methane oxygenate were produced with high H₂O₂ conversions, implying that these are not effective catalysts for this reaction. When CuSO₄ was used as a homogeneous catalyst with a concentration similar to that of Cu/ZSM-5 (entry 6 in Table S2), similar product yields were obtained with the case with Cu/ZSM-5, however, the H₂O₂ conversion was greater than that with Cu/ZSM-5. These results confirm that homogeneous Cu species are not desirable for the selective oxidation of methane into methanol while utilizing H₂O₂ efficiently.

Fe/ZSM-5(IE) showed the highest catalytic activity for the partial oxidation of methane with H₂O₂ at 30 °C and 50 °C in terms of the total product yield among the tested catalysts. However, Fe/ZSM-5(IE) and Cu-Fe/ZSM-5(IE) exhibited similar total product yields normalized to the Fe content for each catalyst, provided the preparation method was the same (Figure S6). This implies that active Fe species can be formed favorably through the IE method and that they are isolated Fe species in the extra-framework of the zeolite. The latter may be detected by UV-Vis spectroscopy. In addition, Fe species that can be probed as Fe²⁺-(NO) by FT-IR spectroscopy after NO adsorption. The promotional effect of the Cu species in Cu-Fe/ZSM-5 on the selective formation of methanol was confirmed. However, the addition of homogeneous Cu species resulted in a lower total product yield but greater H₂O₂ conversion compared to that with only Fe/ZSM-5(IE). This implied that heterogeneous Cu species, which were a highly dispersed Cu²⁺ species, were responsible for the selective formation of methanol. Unfortunately, the Cu species in Cu/ZSM-5 and Cu-Fe/ZSM-5 were unstable under these reaction conditions. Leached Cu was observed after the reaction. Furthermore, Cu leaching caused difficulty for the quantification of HCOOH in the product solution using ¹H-NMR spectroscopy.

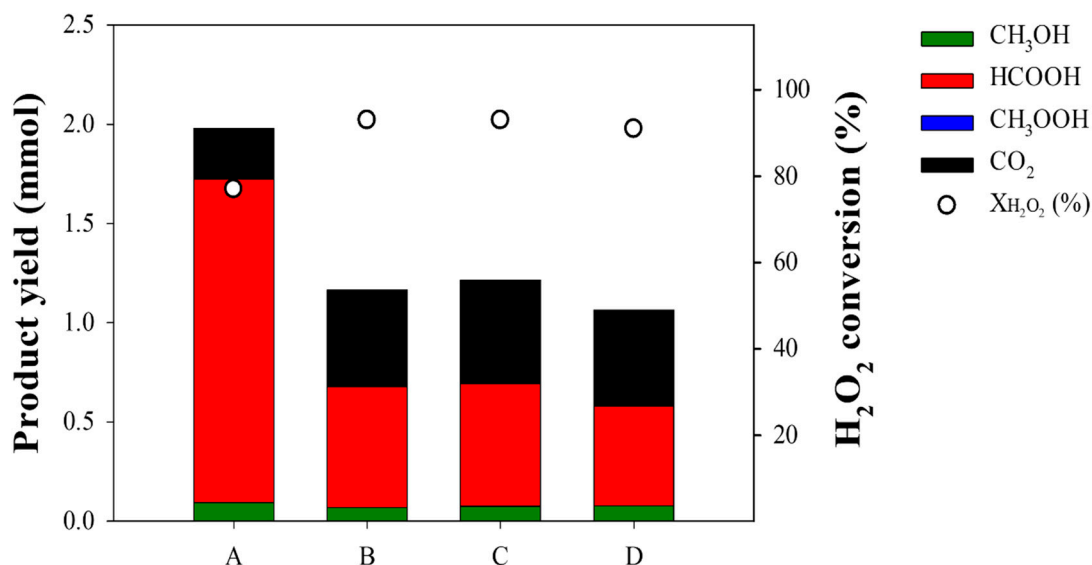


Figure 6. Partial oxidation of methane over 0.51%Fe/ZSM-5(IE) (A), 0.51%Fe/ZSM-5(IE) + Cu(CH₃COO)₂ (B), 0.51%Fe/ZSM-5(IE) + Cu(NO₃)₂ (C), and 0.51%Fe/ZSM-5(IE) + CuSO₄ (D). Reaction conditions: 50 mg catalyst, [Cu] = 0.147 mM, 31 bar methane, 0.277 M H₂O₂, liquid volume = 30 mL, reaction temperature = 50 °C.

Three liquid samples with varying quantities of homogeneous Cu species and formic acid were prepared. The concentration of HCOOH was quantified using ¹H-NMR spectroscopy and HPLC. As shown in Table S3, as the Cu concentration increased from 0.8 to 5.2 ppm, the difference in HCOOH concentration, determined by ¹H-NMR spectroscopy and HPLC, increased. This implied that ¹H-NMR spectroscopy is not suitable for quantifying the HCOOH concentration in the presence of homogeneous Cu species. Copper formate (Cu(HCOO)₂) was chosen as a homogeneous Cu species, and various concentrations of aqueous Cu(HCOO)₂ solutions were prepared. HPLC chromatograms were obtained and compared to those of different HCOOH solution concentrations. Figure S7 shows that the peak area in the HPLC chromatogram was well correlated with the Cu(HCOO)₂ and HCOOH concentrations, which implied that even the concentration of copper formate in water can be accurately quantified by HPLC. Furthermore, a series of standard solutions were prepared and analyzed using ¹H-NMR spectroscopy or HPLC (Figure S8 and Table S4). The presence of H₂O₂ in the standard solution did not inhibit the quantification of HCOOH (Table S4, Entry 2). However, the exact HCOOH concentration could not be determined by ¹H-NMR spectroscopy in the presence of CuSO₄ (entries 3 and 4 in Table S4). The actual HCOOH concentration was measured by HPLC. Therefore, the comparison of HCOOH concentrations in different standard solutions determined by ¹H NMR and HPLC clearly indicated that homogeneous Cu species principally inhibited the quantification of HCOOH concentration by ¹H NMR. These results confirm that the HCOOH concentration cannot be accurately quantified using ¹H-NMR spectroscopy in the presence of homogeneous Cu species. However, there was no difficulty quantifying of HCOOH concentration using HPLC in the absence and presence of homogeneous Cu species. ¹H-NMR spectroscopy has been primarily used to quantify the HCOOH concentration in previous reports on liquid-phase oxidation of methane over Cu-zeolites and Cu-Fe-zeolites [29,38–41,48,49,55,57–64]. This implies that the HCOOH yields reported in previous studies might be underestimated.

The reaction was also performed over Cu-Fe/ZSM-5(IE) at 10, 30, and 50 °C. The total product yield and H₂O₂ conversion increased with increasing reaction temperature (Figure S9). However, the methanol selectivity decreased with increasing reaction temperature. As shown in Table 3, the concentration of leached metal increased with the reaction temperature over Cu-Fe/ZSM-5(IE). It is worth mentioning that the concentration of leached Cu was much greater than that of Fe at the same temperature, which indicated

that the Cu species in the zeolite were most unstable under the reaction conditions. In addition, the effect of HCOOH concentration on Cu leaching was examined over Cu/ZSM-5. The percentage of Cu leached per initial total Cu content increased from 40 to 55% as the concentration of HCOOH increased from 17 to 67 mM (Table S5). This indicated that HCOOH formed during the partial oxidation of methane over Fe species in Fe-containing catalysts was responsible for Cu leaching.

Table 3. The concentration of each metal in the solution after reactions at different temperatures over 0.56%Cu-0.30%Fe/ZSM-5(IE) catalyst ^a.

Entry	Temperature (°C)	Concentration of Each Metal in the Solution (ppm)	
		Cu	Fe
1	10	0.534	0.001
2	30	4.59	0.025
3	50	5.04	0.392

^a Reaction conditions: 30 mL of 0.277 M H₂O₂ solution, 95 mL of CH₄ at 31 bar, 50 mg of catalyst, reaction time = 1 h.

2.3. Catalytic Activity in a Flow Reactor

The continuous liquid-phase selective oxidation of methane was performed in a flow reactor over two active catalysts such as 0.51%Fe/ZSM-5(IE) and 0.56%Cu-0.30%Fe/ZSM-5(IE). H-ZSM-5 was also compared. Their catalytic performance as a function of reaction time is displayed in Figure 7 and Figure S10. The stable catalytic activity in terms of the total product productivity and H₂O₂ conversion was observed over all three catalysts during 12 h of operation. The total product productivity and H₂O₂ conversion decreased in the following order: 0.51%Fe/ZSM-5(IE) > 0.56%Cu-0.30%Fe/ZSM-5(IE) > H-ZSM-5. Note that 0.56%Cu-0.30%Fe/ZSM-5(IE) shows a higher methanol productivity than 0.51%Fe/ZSM-5(IE). These are similar with the results in a batch reactor. It is worth mentioning that the total productivity obtained in this study is higher than those reported previously [65] (Table S6). The concentration of leached Cu species during this continuous operation was analyzed. It was confirmed that the Cu species in 0.56%Cu-0.30%Fe/ZSM-5(IE) were leached continuously as shown in Table S7.

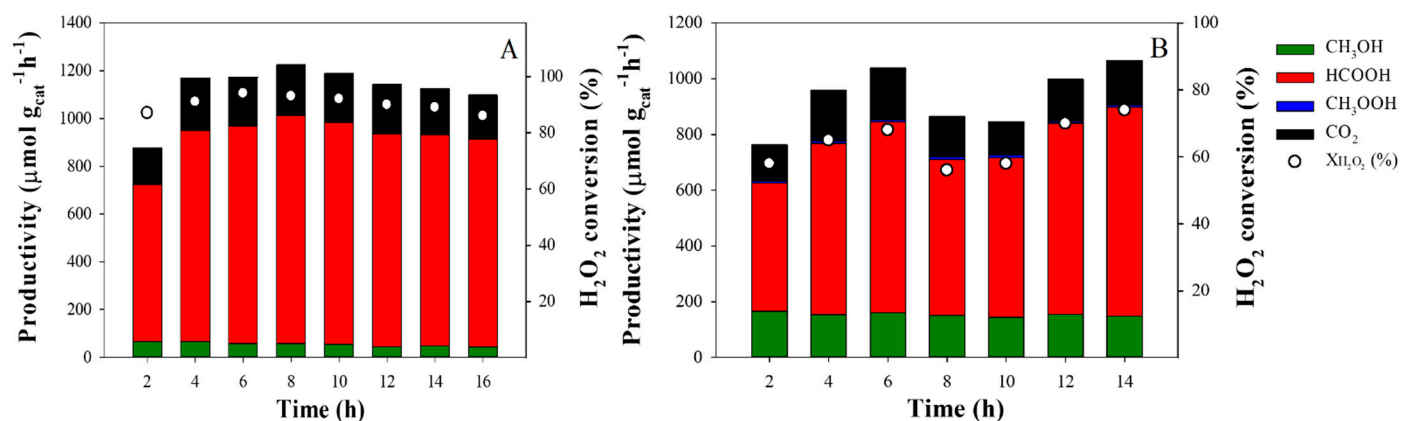


Figure 7. Continuous aqueous phase oxidation of methane with H₂O₂ in a flow reactor over 0.51%Fe/ZSM-5 (A), and 0.56%Cu-0.30%Fe/ZSM-5 (B). Reaction conditions: P_{CH₄} = 21 bar, F_{CH₄} = 50 mL/min, [H₂O₂] = 0.123 mol/L, F_{H₂O₂} = 0.25 mL/min, W_{cat.} = 0.2 g, Temperature = 50 °C.

3. Experiment

3.1. Catalyst Preparation

All the catalysts were prepared from ZSM-5 (CBV 3024E, Zeolyst, Valley Forge, PA, USA), Fe precursors, and Cu precursors using the SIE, WI, and IE methods. ZSM-5 was supplied in the form of ammonium, and its SiO₂/Al₂O₃ ratio was 30.

3.1.1. Solid-State Ion-Exchange (SIE) Method

NH₄-ZSM-5 (3 g) and Cu (II) acetylacetonate (Sigma-Aldrich, St. Louis, MO, USA) and/or Fe (III) acetylacetonate (Sigma-Aldrich, St. Louis, MO, USA), in predetermined quantities, were added to a mortar and mixed for 15 min. The powder was calcined in air at 550 °C for 3 h.

3.1.2. Wet Impregnation (WI) Method

Determined quantities of Cu (II) sulfate pentahydrate (Kanto Chemical, Tokyo, Japan) and/or Fe (II) sulfate heptahydrate (Sigma-Aldrich, St. Louis, MO, USA) were dissolved in 300 mL deionized (DI) water. To this solution, 3 g NH₄-ZSM-5 was added and stirred in a rotary evaporator at 60 rpm at 60 °C for 3 h. After removing the water in vacuum, the recovered powder was dried overnight in an oven at 110 °C and calcined in air at 550 °C for 3 h.

3.1.3. Ion-Exchange (IE) Method

3 g NH₄-ZSM-5 and Cu (II) sulfate pentahydrate (Kanto Chemical, Tokyo, Japan) and/or Fe (II) sulfate heptahydrate (Sigma-Aldrich, St. Louis, MO, USA) were added to 300 mL of a 3.13 mM nitric acid solution and stirred at 80 °C for 2 h in a heating mantle with a magnetic stirrer. The slurry was filtered and washed with deionized water. The recovered powder was dried overnight in an oven at 110 °C, and calcined in air at 550 °C for 3 h.

3.2. Activity Test

Liquid-phase selective oxidation of methane was performed in an autoclave with a total volume of 125 mL. The catalyst (50 mg) was placed in 30 mL of a 0.277 M H₂O₂ solution within a glass liner placed in an autoclave. After sealing the reactor, methane was charged in the reactor to a pressure of 31 bar after purging five times. The autoclave was heated to the target temperature for a reaction time of 1 h. After the reaction, the reactor was rapidly cooled below 10 °C using liquid nitrogen. To determine the effect of homogeneous Cu catalysts, various Cu salts, such as Cu(CH₃COO)₂ (Sigma-Aldrich), Cu(NO₃)₂·3H₂O (Junsei Chemical, Tokyo, Japan), and CuSO₄·5H₂O (Kanto Chemical), were also used. Copper oxides such as CuO (Samchun Chemical, Seoul, Korea) and Cu₂O (Sigma-Aldrich, St. Louis, MO, USA) were used.

Separately, continuous selective oxidation of methane was also conducted in a flow reactor with an internal diameter of 1.27 cm and length of 30 cm. The catalyst (200 mg) was placed on quartz wool packed inside the tubular reactor. 0.123 M H₂O₂ solution and was fed into the reactor with a flowrate of 0.250 mL/min by means of liquid chromatography pump (Lab Alliance series 1500). Methane was also fed into the reactor with a flowrate of 50 mL/min with a mass flow meter (Brooks Instrument, Hatfield, PA, USA). The total pressure was controlled to be 21 bar with a backpressure regulator. The liquid product was collected in the separator, which is maintained at 10 °C with a circulator, just after a reactor and analyzed every 2 h. The gas product was analyzed with online gas chromatograph (GC, Youngin, Anyang, Korea) equipped with a packed column containing Carbosphere (Agilent, Santa Clara, CA, USA) and a flame-ionization detector (FID). A methanizer was used to detect low concentrations of CO₂.

In order to analyze the liquid products, the solution was filtered through a microfilter (Hyundai Micro, Seoul, Korea) and methane oxygenates were quantified with ¹H-NMR using ECZ600R (Jeol, Akishima, Japan) at resonance frequency of ¹H 599.7 MHz with 0.1% trimethylsilylpropanoic acid (TMSO)/D₂O (Euriso-top, Saint Aubin, France) as an external standard. To quantify formic acid content, a high-performance liquid chromatograph with a UV-visible detector (UVD) (Youngin, Anyang, Korea) was used. The liquid products were separated using an Aminex HPX-87H 300 × 7.8 mm (Bio-Rad) column at 35 °C. For the mobile phase, 5 mM sulfuric acid solution was used at a flowrate of 0.6 mL/min. The H₂O₂ concentration was measured using the Ce(SO₄)₂ titration method.

3.3. Catalyst Characterization

N₂ physisorption was performed using a Micromeritics ASAP 2020 (Norcross, GA, USA) instrument to determine the Brunauer–Emmett–Teller (BET) specific surface area, pore volume, pore size, t-plot micropore area, and t-plot micropore volume of the catalyst. Inductively coupled plasma-optical emission spectroscopy (ICP-OES) was performed using an OPTIMA 5300DV (PerkinElmer, Waltham, MA, USA) instrument to determine the metal content of each catalyst and liquid media after the reaction. UV-vis spectra were obtained using a V-650 spectrophotometer (Jasco, Kyoto, Japan) at 200–800 nm with a powder holder. FT-IR experiments were performed on a NICOLET 6700 (Thermo Scientific, Waltham, MA, USA) spectrometer equipped with a mercury cadmium telluride (MCT)-A detector with a ZnSe window in the diffuse reflectance infrared Fourier transform spectroscopy (DRIFTS) cell. The spectra included 16 accumulated scans at a resolution of 3.857 cm⁻¹. Before NO adsorption, the sample was heated to 500 °C for 10 min in He and cooled to room temperature. NO adsorption was performed for 20 min at 30 °C by flowing feed gas composed of 5000 ppm NO in He at a flow rate of 20 mL/min. The temperature-programmed reduction with H₂ (H₂-TPR) was conducted using a Micromeritics 2920 Autochem instrument (Norcross, GA, USA). A sample of 100 mg was loaded in a quartz tube, and the temperature was increased from 30 to 900 °C at a heating rate of 10 °C/min under a flow of 10 mol% H₂/Ar while monitoring the thermal conductivity detector. X-ray diffraction (XRD) patterns were obtained by a Rigaku D/Max instrument (Tokyo, Japan) with a Cu K α source to assess the bulk crystalline structure of the samples. Transmission electron microscopy (JEM-3010, JEOL Ltd., Akishima, Japan) with energy-dispersive X-ray spectroscopy (EDS, Oxford instrument, Abingdon, UK) was used to find out if there is any metal oxide clusters in the catalysts.

4. Conclusions

The promotional effect of the Cu species in Cu-Fe/ZSM-5 on selective methanol formation during the aqueous-phase partial oxidation of methane with H₂O₂ was confirmed. However, observable quantities of Cu species leached from Cu-Fe/ZSM-5 and Cu/ZSM-5. These leached Cu species interfere with the quantification of HCOOH with ¹H-NMR. The formation of HCOOH was confirmed over Cu-Fe/ZSM-5 using an HPLC analysis which was not affected by the presence of leached homogeneous Cu species. Homogeneous Cu species adversely affected the catalytic performance of Fe/ZSM-5 by decreasing the product yield of methane oxygenates and increasing H₂O₂ conversion. The ion-exchange method is the best method for providing highly dispersed Cu²⁺ and Fe²⁺ species in Cu-Fe/ZSM-5 and Fe/ZSM-5 among the wet-impregnation, solid-state ion-exchange, and ion-exchange methods.

Supplementary Materials: The following supporting information can be downloaded at: <https://www.mdpi.com/article/10.3390/catal12101224/s1>, Figure S1. N₂ adsorption and desorption isotherm of the prepared catalyst. Figure S2. XRD patterns of the prepared catalysts. Figure S3. TEM images and EDS mapping results for the prepared catalysts. Figure S4. Deconvolution of UV-Vis spectra for the catalysts prepared with different methods. Figure S5. NO-FTIR spectra for the catalysts prepared with different methods from 0 to 20 min. Figure S6. Partial oxidation of methane over Cu-Fe/ZSM-5(SIE) (A), Cu-Fe/ZSM-5(WI) (B), Cu-Fe/ZSM-5(IE) (C), Fe/ZSM-5(SIE) (D), Fe/ZSM-5(WI) (E), and Fe/ZSM-5(IE) (F). Figure S7. HPLC chromatograms for the standard solutions of different HCOOH and Cu(HCOO)₂ concentrations. Figure S8. HPLC chromatograms for the standard solutions with different compositions. Figure S9. Partial oxidation of methane over Cu-Fe/ZSM-5(IE) catalyst at different temperatures. Figure S10. Continuous aqueous phase oxidation of methane with H₂O₂ in a flow reactor over H-ZSM-5. Table S1. The fraction of each Fe species estimated from the UV-vis band in Figure S3 for Fe/ZSM-5 and Cu-Fe/ZSM-5 catalysts. Table S2. Catalytic activity result of partial oxidation of methane in this study at 50 °C. Table S3. The Cu concentration in the product solution, ¹H-NMR spectra, and concentrations of HCOOH determined with ¹H-NMR and HPLC during the cyclic test. Table S4. Concentrations of HCOOH in different stand solutions determined with ¹H-NMR and HPLC. Table S5. The amount of Cu leached from Cu/ZSM-5 with

different concentrations of HCOOH. Table S6. The activity comparison among catalysts reported previously and in this work during continuous liquid-phase selective oxidation of methane in a flow reactor. Table S7. The concentration of Cu species in the product solution during continuous liquid-phase selective oxidation of methane over 0.56%Cu-0.30%Fe/ZSM-5(IE) in a flow reactor.

Author Contributions: M.S.K. and G.S.Y.: experimental investigation and data analysis, writing—original draft preparation; E.D.P.: supervision, writing—review and editing, project administration, funding acquisition. All authors have read and agreed to the published version of the manuscript.

Funding: This work was supported by the C1 Gas Refinery Program through the National Research Foundation of Korea (NRF), funded by the Ministry of Science and ICT and Future Planning (2015M3D3A1A01064899).

Conflicts of Interest: The authors declare no conflict of interest.

References

1. Cheng, K.; Kang, J.; King, D.L.; Subramanian, V.; Zhou, C.; Zhang, Q.; Wang, Y. Chapter Three—Advances in Catalysis for Syngas Conversion to Hydrocarbons. In *Advances in Catalysis*; Song, C., Ed.; Academic Press: Cambridge, MA, USA, 2017; Volume 60, pp. 125–208.
2. Siirola, J.J. The impact of shale gas in the chemical industry. *AIChE J.* **2014**, *60*, 810–819. [[CrossRef](#)]
3. Tang, P.; Zhu, Q.; Wu, Z.; Ma, D. Methane activation: The past and future. *Energy Environ. Sci.* **2014**, *7*, 2580–2591. [[CrossRef](#)]
4. Olivos-Suarez, A.I.; Szécsényi, Á.; Hensen, E.J.M.; Ruiz-Martinez, J.; Pidko, E.A.; Gascon, J. Strategies for the Direct Catalytic Valorization of Methane Using Heterogeneous Catalysis: Challenges and Opportunities. *ACS Catal.* **2016**, *6*, 2965–2981. [[CrossRef](#)]
5. Schwach, P.; Pan, X.; Bao, X. Direct Conversion of Methane to Value-Added Chemicals over Heterogeneous Catalysts: Challenges and Prospects. *Chem. Rev.* **2017**, *117*, 8497–8520. [[CrossRef](#)]
6. Sun, L.; Wang, Y.; Guan, N.; Li, L. Methane Activation and Utilization: Current Status and Future Challenges. *Energy Technol.* **2020**, *8*, 1900826. [[CrossRef](#)]
7. Ravi, M.; Ranocchiari, M.; van Bokhoven, J.A. The Direct Catalytic Oxidation of Methane to Methanol—A Critical Assessment. *Angew. Chem. Int. Ed.* **2017**, *56*, 16464–16483. [[CrossRef](#)]
8. Taifan, W.; Baltrusaitis, J. CH₄ conversion to value added products: Potential, limitations and extensions of a single step heterogeneous catalysis. *Appl. Catal. B* **2016**, *198*, 525–547. [[CrossRef](#)]
9. Kondratenko, E.V.; Peppel, T.; Seeburg, D.; Kondratenko, V.A.; Kalevaru, N.; Martin, A.; Wohlrab, S. Methane conversion into different hydrocarbons or oxygenates: Current status and future perspectives in catalyst development and reactor operation. *Catal. Sci. Technol.* **2017**, *7*, 366–381. [[CrossRef](#)]
10. Hammond, C.; Conrad, S.; Hermans, I. Oxidative Methane Upgrading. *ChemSusChem* **2012**, *5*, 1668–1686. [[CrossRef](#)]
11. Xu, Z.C.; Park, E.D. Gas-Phase Selective Oxidation of Methane into Methane Oxygenates. *Catalysts* **2022**, *12*, 314. [[CrossRef](#)]
12. Gunsalus, N.J.; Koppaka, A.; Park, S.H.; Bischof, S.M.; Hashiguchi, B.G.; Periana, R.A. Homogeneous Functionalization of Methane. *Chem. Rev.* **2017**, *117*, 8521–8573. [[CrossRef](#)] [[PubMed](#)]
13. Zimmermann, T.; Soorholtz, M.; Bilke, M.; Schüth, F. Selective Methane Oxidation Catalyzed by Platinum Salts in Oleum at Turnover Frequencies of Large-Scale Industrial Processes. *J. Am. Chem. Soc.* **2016**, *138*, 12395–12400. [[CrossRef](#)] [[PubMed](#)]
14. Dang, H.T.; Lee, H.W.; Lee, J.; Choo, H.; Hong, S.H.; Cheong, M.; Lee, H. Enhanced Catalytic Activity of (DMSO)₂PtCl₂ for the Methane Oxidation in the SO₃–H₂SO₄ System. *ACS Catal.* **2018**, *8*, 11854–11862. [[CrossRef](#)]
15. Zhang, Y.; Zhang, M.; Han, Z.; Huang, S.; Yuan, D.; Su, W. Atmosphere-Pressure Methane Oxidation to Methyl Trifluoroacetate Enabled by a Porous Organic Polymer-Supported Single-Site Palladium Catalyst. *ACS Catal.* **2021**, *11*, 1008–1013. [[CrossRef](#)]
16. Zimmermann, T.; Bilke, M.; Soorholtz, M.; Schüth, F. Influence of Catalyst Concentration on Activity and Selectivity in Selective Methane Oxidation with Platinum Compounds in Sulfuric Acid and Oleum. *ACS Catal.* **2018**, *8*, 9262–9268. [[CrossRef](#)]
17. Hashiguchi, B.G.; Bischof, S.M.; Konnick, M.M.; Periana, R.A. Designing Catalysts for Functionalization of Unactivated C–H Bonds Based on the CH Activation Reaction. *Acc. Chem. Res.* **2012**, *45*, 885–898. [[CrossRef](#)] [[PubMed](#)]
18. Lee, H.W.; Dang, H.T.; Kim, H.; Lee, U.; Ha, J.-M.; Jae, J.; Cheong, M.; Lee, H. Pt black catalyzed methane oxidation to methyl bisulfate in H₂SO₄–SO₃. *J. Catal.* **2019**, *374*, 230–236. [[CrossRef](#)]
19. Ravi, M.; Bokhoven, J. Homogeneous Copper-Catalyzed Conversion of Methane to Methyl Trifluoroacetate in High Yield at Low Pressure. *ChemCatChem* **2018**, *10*, 2383–2386. [[CrossRef](#)]
20. Blankenship, A.N.; Ravi, M.; Newton, M.A.; van Bokhoven, J.A. Heterogeneously Catalyzed Aerobic Oxidation of Methane to a Methyl Derivative. *Angew. Chem. Int. Ed.* **2021**, *60*, 18138–18143. [[CrossRef](#)]
21. Freakley, S.J.; Dimitratos, N.; Willock, D.J.; Taylor, S.H.; Kiely, C.J.; Hutchings, G.J. Methane Oxidation to Methanol in Water. *Acc. Chem. Res.* **2021**, *54*, 2614–2623. [[CrossRef](#)] [[PubMed](#)]
22. Wang, V.; Maji, S.; Chen, P.; Lee, H.; Yu, S.; Chan, S. Alkane Oxidation: Methane Monooxygenases, Related Enzymes, and Their Biomimetics. *Chem. Rev.* **2017**, *117*, 8574–8621. [[CrossRef](#)] [[PubMed](#)]
23. Snyder, B.E.R.; Bols, M.L.; Schoonheydt, R.A.; Sels, B.F.; Solomon, E.I. Iron and Copper Active Sites in Zeolites and Their Correlation to Metalloenzymes. *Chem. Rev.* **2018**, *118*, 2718–2768. [[CrossRef](#)] [[PubMed](#)]

24. Sheldon, R.A.; Arends, I.W.C.E.; Lempers, H.E.B. Liquid phase oxidation at metal ions and complexes in constrained environments. *Catal. Today* **1998**, *41*, 387–407. [[CrossRef](#)]
25. Sarkar, S.; Moser, M.L.; Tian, X.; Zhang, X.; Al-Hadeethi, Y.F.; Haddon, R.C. Metals on Graphene and Carbon Nanotube Surfaces: From Mobile Atoms to Atomtronics to Bulk Metals to Clusters and Catalysts. *Chem. Mater.* **2014**, *26*, 184–195. [[CrossRef](#)]
26. Jiao, L.; Wang, Y.; Jiang, H.-L.; Xu, Q. Metal–Organic Frameworks as Platforms for Catalytic Applications. *Adv. Mater.* **2018**, *30*, 1703663. [[CrossRef](#)] [[PubMed](#)]
27. Ohyama, J.; Hirayama, A.; Kondou, N.; Yoshida, H.; Machida, M.; Nishimura, S.; Hirai, K.; Miyazato, I.; Takahashi, K. Data science assisted investigation of catalytically active copper hydrate in zeolites for direct oxidation of methane to methanol using H₂O₂. *Sci. Rep.* **2021**, *11*, 2067. [[CrossRef](#)] [[PubMed](#)]
28. Jin, Z.; Wang, L.; Zuidema, E.; Mondal, K.; Zhang, M.; Zhang, J.; Wang, C.; Meng, X.; Yang, H.; Mesters, C.; et al. Hydrophobic zeolite modification for in situ peroxide formation in methane oxidation to methanol. *Science* **2020**, *367*, 193–197. [[CrossRef](#)] [[PubMed](#)]
29. Szécsényi, Á.; Li, G.; Gascon, J.; Pidko, E.A. Mechanistic Complexity of Methane Oxidation with H₂O₂ by Single-Site Fe/ZSM-5 Catalyst. *ACS Catal.* **2018**, *8*, 7961–7972. [[CrossRef](#)]
30. He, Y.; Liang, J.; Imai, Y.; Ueda, K.; Li, H.; Guo, X.; Yang, G.; Yoneyama, Y.; Tsubaki, N. Highly selective synthesis of methanol from methane over carbon materials supported Pd–Au nanoparticles under mild conditions. *Catal. Today* **2020**, *352*, 104–110. [[CrossRef](#)]
31. Hong, S.; Mpourmpakis, G. Mechanistic understanding of methane-to-methanol conversion on graphene-stabilized single-atom iron centers. *Catal. Sci. Technol.* **2021**, *11*, 6390–6400. [[CrossRef](#)]
32. Cui, X.; Li, H.; Wang, Y.; Hu, Y.; Hua, L.; Li, H.; Han, X.; Liu, Q.; Yang, F.; He, L.; et al. Room-Temperature Methane Conversion by Graphene-Confined Single Iron Atoms. *Chem* **2018**, *4*, 1902–1910. [[CrossRef](#)]
33. Tan, X.; Tahini, H.A.; Smith, S.C. Defect Engineering in Graphene-Confined Single-Atom Iron Catalysts for Room-Temperature Methane Conversion. *J. Phys. Chem. C* **2021**, *125*, 12628–12635. [[CrossRef](#)]
34. Kholdeeva, O.; Maksimchuk, N. Metal–Organic Frameworks in Oxidation Catalysis with Hydrogen Peroxide. *Catalysts* **2021**, *11*, 283. [[CrossRef](#)]
35. Yarulina, I.; Chowdhury, A.D.; Meirer, F.; Weckhuysen, B.M.; Gascon, J. Recent trends and fundamental insights in the methanol-to-hydrocarbons process. *Nat. Catal.* **2018**, *1*, 398–411. [[CrossRef](#)]
36. Kianfar, E.; Hajimirzaee, S.; mousavian, S.; Mehr, A.S. Zeolite-based catalysts for methanol to gasoline process: A review. *Microchem. J.* **2020**, *156*, 104822. [[CrossRef](#)]
37. Kalck, P.; Le Berre, C.; Serp, P. Recent advances in the methanol carbonylation reaction into acetic acid. *Coord. Chem. Rev* **2020**, *402*, 213078. [[CrossRef](#)]
38. Hammond, C.; Forde, M.M.; Ab Rahim, M.H.; Thetford, A.; He, Q.; Jenkins, R.L.; Dimitratos, N.; Lopez-Sanchez, J.A.; Dummer, N.F.; Murphy, D.M.; et al. Direct Catalytic Conversion of Methane to Methanol in an Aqueous Medium by using Copper-Promoted Fe-ZSM-5. *Angew. Chem. Int. Ed.* **2012**, *51*, 5129–5133. [[CrossRef](#)]
39. Al-Shihri, S.; Richard, C.J.; Al-Megren, H.; Chadwick, D. Insights into the direct selective oxidation of methane to methanol over ZSM-5 zeolites in aqueous hydrogen peroxide. *Catal. Today* **2020**, *353*, 269–278. [[CrossRef](#)]
40. Yu, T.; Li, Z.; Lin, L.; Chu, S.; Su, Y.; Song, W.; Wang, A.; Weckhuysen, B.M.; Luo, W. Highly Selective Oxidation of Methane into Methanol over Cu-Promoted Monomeric Fe/ZSM-5. *ACS Catal.* **2021**, *11*, 6684–6691. [[CrossRef](#)]
41. Forde, M.M.; Armstrong, R.D.; McVicker, R.; Wells, P.P.; Dimitratos, N.; He, Q.; Lu, L.; Jenkins, R.L.; Hammond, C.; Lopez-Sanchez, J.A.; et al. Light alkane oxidation using catalysts prepared by chemical vapour impregnation: Tuning alcohol selectivity through catalyst pre-treatment. *Chem. Sci.* **2014**, *5*, 3603–3616. [[CrossRef](#)]
42. Forde, M.M.; Armstrong, R.D.; Hammond, C.; He, Q.; Jenkins, R.L.; Kondrat, S.A.; Dimitratos, N.; Lopez-Sanchez, J.A.; Taylor, S.H.; Willock, D.; et al. Partial Oxidation of Ethane to Oxygenates Using Fe- and Cu-Containing ZSM-5. *J. Am. Chem. Soc.* **2013**, *135*, 11087–11099. [[CrossRef](#)] [[PubMed](#)]
43. Praliaud, H.; Mikhailenko, S.D.; Chajar, Z.; Primet, M. Surface and bulk properties of Cu-ZSM-5 and Cu/Al₂O₃ solids during redox treatments. Correlation with the selective reduction of nitric oxide by hydrocarbons. *Appl. Catal. B* **1998**, *16*, 359–374. [[CrossRef](#)]
44. Wichterlová, B.; Dědeček, J.; Sobalík, Z.; Vondrová, A.; Klier, K. On the Cu Site in ZSM-5 Active in Decomposition of NO: Luminescence, FTIR Study, and Redox Properties. *J. Catal.* **1997**, *169*, 194–202. [[CrossRef](#)]
45. Jouini, H.; Mejri, I.; Petitto, C.; Martinez-Ortigosa, J.; Vidal-Moya, A.; Mhamdi, M.; Blasco, T.; Delahay, G. Characterization and NH₃-SCR reactivity of Cu-Fe-ZSM-5 catalysts prepared by solid state ion exchange: The metal exchange order effect. *Microporous Mesoporous Mater.* **2018**, *260*, 217–226. [[CrossRef](#)]
46. Heinrich, F.; Schmidt, C.; Löffler, E.; Menzel, M.; Grünert, W. Fe-ZSM-5 Catalysts for the Selective Reduction of NO by Isobutane—The Problem of the Active Sites. *J. Catal.* **2002**, *212*, 157–172. [[CrossRef](#)]
47. Delahay, G.; Guzman-Vargas, A.; Valade, D.; Coq, B. Selective Catalytic Reduction of no by NH₃ on Fe-ZSM-5 Elaborated from Different Methods. *Stud. Surf. Sci. Catal.* **2004**, *154 C*, 2501–2508. [[CrossRef](#)]
48. Kim, M.S.; Park, E.D. Aqueous-phase partial oxidation of methane with H₂O₂ over Fe-ZSM-5 catalysts prepared from different iron precursors. *Microporous Mesoporous Mater.* **2021**, *324*, 111278. [[CrossRef](#)]

49. Kim, M.S.; Park, K.H.; Cho, S.J.; Park, E.D. Partial oxidation of methane with hydrogen peroxide over Fe-ZSM-5 catalyst. *Catal. Today* **2021**, *376*, 113–118. [[CrossRef](#)]
50. Hadjiivanov, K.; Saussey, J.; Freysz, J.L.; Lavalley, J.C. FT-IR study of NO + O₂ co-adsorption on H-ZSM-5: Re-assignment of the 2133 cm⁻¹ band to NO⁺ species. *Catal. Lett.* **1998**, *52*, 103–108. [[CrossRef](#)]
51. Lobree, L.J.; Hwang, I.C.; Reimer, J.A.; Bell, A.T. Investigations of the State of Fe in H ZSM-5. *J. Catal.* **1999**, *186*, 242–253. [[CrossRef](#)]
52. Lezcano, M.; Kovalchuk, V.I.; D'itri, J.L. FTIR Study of the Interaction of Nitric Oxide with Fe-ZSM-5. *Kinet. Catal.* **2001**, *42*, 104–111. [[CrossRef](#)]
53. Mul, G.; Pérez-Ramírez, J.; Kapteijn, F.; Moulijn, J.A. NO Adsorption on Ex-Framework [Fe,X]MFI Catalysts: Novel IR Bands and Evaluation of Assignments. *Catal. Lett.* **2002**, *80*, 129–138. [[CrossRef](#)]
54. Giordanino, F.; Vennestrøm, P.N.R.; Lundegaard, L.F.; Stappen, F.N.; Mossin, S.; Beato, P.; Bordiga, S.; Lamberti, C. Characterization of Cu-exchanged SSZ-13: A comparative FTIR, UV-Vis, and EPR study with Cu-ZSM-5 and Cu-β with similar Si/Al and Cu/Al ratios. *Dalton Trans.* **2013**, *42*, 12741–12761. [[CrossRef](#)] [[PubMed](#)]
55. Armstrong, R.D.; Peneau, V.; Ritterskamp, N.; Kiely, C.J.; Taylor, S.H.; Hutchings, G.J. The Role of Copper Speciation in the Low Temperature Oxidative Upgrading of Short Chain Alkanes over Cu/ZSM-5 Catalysts. *ChemPhysChem* **2018**, *19*, 469–478. [[CrossRef](#)] [[PubMed](#)]
56. Dedecek, J.; Čapek, L.; Sazama, P.; Sobalik, Z.; Wichterlová, B. Control of metal ion species in zeolites by distribution of aluminium in the framework: From structural analysis to performance under real conditions of SCR-NO_x and NO, N₂O decomposition. *Appl. Catal. A* **2011**, *391*, 244–253. [[CrossRef](#)]
57. Li, G.; Pidko, E.A.; van Santen, R.A.; Li, C.; Hensen, E.J.M. Stability of Extraframework Iron-Containing Complexes in ZSM-5 Zeolite. *J. Phys. Chem. C* **2013**, *117*, 413–426. [[CrossRef](#)]
58. Hammond, C.; Dimitratos, N.; Jenkins, R.L.; Lopez-Sanchez, J.A.; Kondrat, S.A.; Hasbi ab Rahim, M.; Forde, M.M.; Thetford, A.; Taylor, S.H.; Hagen, H.; et al. Elucidation and Evolution of the Active Component within Cu/Fe/ZSM-5 for Catalytic Methane Oxidation: From Synthesis to Catalysis. *ACS Catal.* **2013**, *3*, 689–699. [[CrossRef](#)]
59. Hammond, C.; Dimitratos, N.; Lopez-Sanchez, J.A.; Jenkins, R.L.; Whiting, G.; Kondrat, S.A.; ab Rahim, M.H.; Forde, M.M.; Thetford, A.; Hagen, H.; et al. Aqueous-Phase Methane Oxidation over Fe-MFI Zeolites; Promotion through Isomorphous Framework Substitution. *ACS Catal.* **2013**, *3*, 1835–1844. [[CrossRef](#)]
60. Armstrong, R.D.; Freakley, S.J.; Forde, M.M.; Peneau, V.; Jenkins, R.L.; Taylor, S.H.; Moulijn, J.A.; Morgan, D.J.; Hutchings, G.J. Low temperature catalytic partial oxidation of ethane to oxygenates by Fe- and Cu-ZSM-5 in a continuous flow reactor. *J. Catal.* **2015**, *330*, 84–92. [[CrossRef](#)]
61. Kalamaras, C.; Palomas, D.; Bos, R.; Horton, A.; Crimmin, M.; Hellgardt, K. Selective Oxidation of Methane to Methanol Over Cu- and Fe-Exchanged Zeolites: The Effect of Si/Al Molar Ratio. *Catal. Lett.* **2016**, *146*, 483–492. [[CrossRef](#)]
62. Peneau, V.; Armstrong, R.D.; Shaw, G.; Xu, J.; Jenkins, R.L.; Morgan, D.J.; Dimitratos, N.; Taylor, S.H.; Zanthoff, H.W.; Peitz, S.; et al. The Low-Temperature Oxidation of Propane by using H₂O₂ and Fe/ZSM-5 Catalysts: Insights into the Active Site and Enhancement of Catalytic Turnover Frequencies. *ChemCatChem* **2017**, *9*, 642–650. [[CrossRef](#)]
63. Xiao, P.; Wang, Y.; Nishitoba, T.; Kondo, J.N.; Yokoi, T. Selective oxidation of methane to methanol with H₂O₂ over an Fe-MFI zeolite catalyst using sulfolane solvent. *Chem. Commun.* **2019**, *55*, 2896–2899. [[CrossRef](#)]
64. Yashnik, S.A.; Boltenkov, V.V.; Babushkin, D.E.; Taran, O.P.; Parmon, V.N. Methane Oxidation by H₂O₂ over Different Cu-Species of Cu-ZSM-5 Catalysts. *Top. Catal.* **2020**, *63*, 203–221. [[CrossRef](#)]
65. Xu, J.; Armstrong, R.D.; Shaw, G.; Dummer, N.F.; Freakley, S.J.; Taylor, S.H.; Hutchings, G.J. Continuous selective oxidation of methane to methanol over Cu- and Fe-modified ZSM-5 catalysts in a flow reactor. *Catal. Today* **2016**, *270*, 93–100. [[CrossRef](#)]